Journal of the Optical Society of America B

OPTICAL PHYSICS

Fast and low grating lobe multi-beam steering with a subarray level unequally spaced optical phased array

YUNHAN WU,[1,2] SHUAI SHAO,[1,*] AND DONGBO CHE[1,2]

[1]State Key Laboratory of Laser Interaction with Matter, Changchun Institute of Optics, Fine Mechanics and Physics, Chinese Academy of Sciences, Changchun 130033, China
[2]University of Chinese Academy of Sciences, Beijing 100049, China
*Corresponding author: sshuaiciomp2021@163.com

Received 23 June 2021; revised 15 September 2021; accepted 15 September 2021; posted 17 September 2021 (Doc. ID 434347); published 22 October 2021

A grating-lobe-suppressed optical phased array (OPA) based on an unequally spaced technique is proposed to realize multi-beam steering, in which the multi-beam is achieved using the subaperture (SA) technique. The element distribution in SA is optimized by a modified genetic algorithm to minimize peak sidelobe levels (PSLL). The results show that grating lobes can be well suppressed using the proposed technique within the whole scanning range of the beams. The PSLL of the optimized unequally spaced OPA reaches as low as 0.21 in the ±5° beam direction, which is much better than the equally spaced OPA. Simultaneously, multi-beam asynchronous scanning can be achieved, which significantly improves the accuracy and flexibility of beam steering control. Besides, the simulations show that the spacing range between adjacent elements and the element number should be appropriately chosen to achieve better sidelobe suppression and a narrow beam width.

https://doi.org/10.1364/JOSAB.434347

1. INTRODUCTION

Optical beam steering [1,2] is widely applied in light detection and ranging (LIDAR), free space optical communication, and optical microscopy [3–5]. Compared to other beam steering techniques, such as mechanical beam steering and electro-optical beam steering [4,6–10], an optical phased array (OPA) [11] is a promising optical beam steering technique that enables accurate and rapid beam steering without the inertia of mechanical motion. The advantages of applying OPA to beam steering include high resolution, chip scale, light weight, high scanning speed, and programmable multiple beam random-access pointing [12,13]. However, limited by the fabrication levels, the minimum of the element spacing of an OPA is much larger than half of the light wavelength, which causes grating lobes in the far field [2,3,14–16]. The appearance of large grating lobes would not only disperse radiation energy and reduce gain but also misjudge the target location and should be suppressed. Thus, grating lobes pose a great challenge for the OPA technology [17], and it is necessary to eliminate or reduce their effect.

Some research indicates that a non-periodic distribution of elements enables the suppression of grating lobes [18,19]. For example, unequally spaced OPA can overcome the limit of half the wavelength, meet the requirements of existing optical processing techniques, and reduce or eliminate grating lobes' effects. Some optimization algorithms, such as particle swarm algorithms (FSO) [20] and genetic algorithms (GA) [21], are employed to achieve optical phased array element spacing arrangements to reduce the grating lobe level. Single-beam scanning modality has been demonstrated in LIDAR systems by using mechanical steering devices or OPA. Scanning multiple beams can help reduce the scanning angle, ensure a wide field of view (FOV), and improve the frame rate [22]. Several methods have been proposed to generate multi-beams. The most straightforward implementation is cascading a sequence of OPAs directly; however, insertion loss will be accumulated, and the number of beams is limited. Another method is to employ computer generated holograms on liquid crystal spatial light modulators to produce multiple beams. Nevertheless, this method usually requires a comparatively long simulation time to complete the complicated calculations [23,24]. The last method, the "subaperture array" method, can form multiple independent beams using independently programmed subapertures (SAs). The multi-beam emitting OPA can provide an M-beam array, which covers a wide angular range and is steerable in one dimension to get a higher spatial resolution [25]. The whole aperture of an OPA can be divided into M subapertures. Each one is a subaperture that can be separately managed and independently controlled. M subapertures have the ability to form M independent steering beams theoretically. Although the sidelobes can be well suppressed for the element

distribution, the sidelobes' level may rise once the desired beam direction changes. This is caused by the asymmetrical structure of the OPA. Therefore, to achieve wide-angle beam steering, the element spacing of the OPA should be continually optimized to ensure that the sidelobes are well suppressed. This increases the complexity of the system and limits the beam steering angle.

In this paper, we propose and numerically investigate a subarray level aperiodic multi-beam array to implement fast and wide-range optical beam steering. Using the modified genetic algorithm, the distribution of the phased array elements can be quickly optimized to largely suppress the grating lobes and side lobes. The optimized OPA implements wide-angle multi-beam steering without reconfiguring the OPA element distribution, and the PSLL can be kept in a low range. Besides the good sidelobe suppression capability, another advantage of the optimized OPA is that optical beam asynchronous steering in a wide scanning range can be achieved. In this study, the performance of the proposed OPA is investigated and analyzed through numerical simulation. The relationship between PSLL and scanning ranges is also investigated for different the number of elements.

2. PRINCIPLE

A. Phased-Array Beamforming Principle

Phased-array technology is based on the principle that electromagnetic waves interfere with each other in space. Figure 1 gives a schematic diagram of a typical uniform OPA for single-beam steering. Considering a linear array with N elements, the near-field radiation field amplitude on the ith ($i = 0, 1, 2, \cdots, N-1$) array element is A_i. The electric field intensity of the ith element is $E_i(\theta)$, and the distance between element i and the far-field observation point is r_i. Assuming that the physical dimensions of array elements are ignored, it is a point source with omnidirectional radiation. Then the total electric field intensity can be expressed as [25,26]

$$E(\theta) = \sum_{i=0}^{N-1} E_i(\theta) = \sum_{i=0}^{N-1} A_i e^{-ij\Delta\Phi} \frac{e^{-jkr_i}}{r_i}, \tag{1}$$

where $k = \frac{2\pi}{\lambda}$, λ is the wavelength, and the spacing between every two adjacent elements is d. The phase difference between adjacent elements is $\Delta\Phi$.

We define

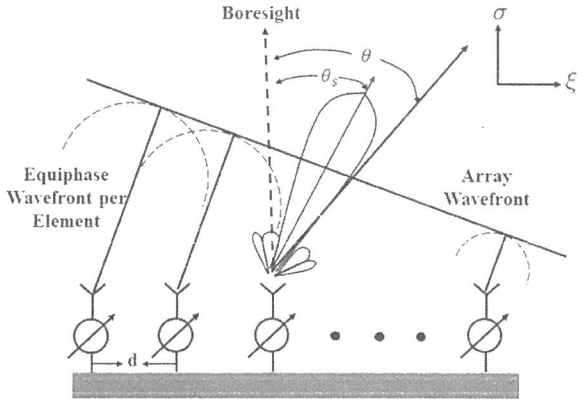

Fig. 1. Diagram of a uniform linear array.

$$\begin{cases} r_i = r_0 - id\sin\theta \\ \Delta\Phi = kd\sin\theta_s \end{cases}, \tag{2}$$

where θ and θ_s denote the observation direction and the beam direction angle, respectively. $\Delta\Phi_e$ is the phase difference introduced by the spatially distributed position of each array element. Then Eq. (2) can be rewritten as

$$E(\theta) = \frac{e^{-jkr_0}}{r_0} \bullet \sum_{i=0}^{N-1} A_i e^{-ij(\Delta\Phi_e - \Delta\Phi)}. \tag{3}$$

For the optical phased-array far-field electric field intensity, we are only concerned with its relative distribution, ignoring amplitude and phase [no contributing constant terms in Eq. (3)]. We further assume that amplitude is the same for all phase elements. Equation (2) can be simplified as

$$E(\theta) = \frac{\sin\left[\frac{N}{2}kd(\sin\theta - \sin\theta_s)\right]}{\sin\left[\frac{1}{2}kd(\sin\theta - \sin\theta_s)\right]}. \tag{4}$$

The direction of the main lobe is at $\theta_s = \theta$. By controlling the initial phase distribution among the elements that determine θ, which is the foundation for beam steering using phased array technology, the locations of grating lobes in single beam steering are determined by

$$\frac{\pi d(\sin\theta - \sin\theta_s)}{\lambda} = \pm\pi, \pm 2\pi, \pm 3\pi, \cdots. \tag{5}$$

Note that this condition can be easily satisfied in the microwave region due to the long wavelength. To ensure the efficiency of light propagation, the feature sizes of the optical wavelength or fibers are much larger than half the wavelength. In practice, grating lobes appear if the pixel size is not subwavelength, which is an issue for many optical technologies.

B. Multiple-Beam Forming Methods

In multi-beam forming technology, the array aperture is large relative to the wavelength and can be divided into many subarrays. Dividing the whole aperture into M segments, each of these M apertures have m elements, and all the small apertures have phase-shift differences expressed as $\Delta\Phi_1, \Delta\Phi_2, \cdots, \Delta\Phi_M$. The far-field amplitude distribution of the phase modulated is as follows:

$$E_{SA}(\theta) = \sum_{n=0}^{m-1} e^{jnd\frac{\pi}{\lambda}(\sin\theta - \sin\theta_1)} + \sum_{n=m}^{2m-1} e^{jnd\frac{\pi}{\lambda}(\sin\theta - \sin\theta_2)} + \cdots + \sum_{n=(M-1)m}^{Mm-1} e^{jnd\frac{\pi}{\lambda}(\sin\theta - \sin\theta_M)}, \tag{6}$$

where θ_M is the main lobe of the Mth beam, corresponding to the phase shift difference $\Delta\Phi_M$. Comparing Eq. (1), the element factor of these two equations has changed, that is, the equivalent element spacing of each beam in the multi-beam steering is M times larger than the original spacing. Relatively speaking, it is easier to achieve grating lobes in beam steering.

Next, we calculate the far-field electric field distribution of N elements located in the $x - y$ plane. The coordinate of the nth

element is (x_n, y_n). We apply the Fraunhofer far-field approximation and calculate the far-field diffraction pattern observed in the plane $\sigma - \zeta$ using

$$E(\sigma,\zeta) = \int_{\infty}^{-\infty}\int_{\infty}^{-\infty}\sum_{n=0}^{N} A_n e^{j\Phi_n} \times e^{\left[-j\frac{k}{L}(x\sigma+y\zeta)\right]}dxdy$$

$$= \sum_{n=0}^{N} A_n e^{j\Phi_n} \times e^{\left[-j\frac{k}{L}(x\sigma+y\zeta)\right]}dxdy. \quad (7)$$

In Eq. (6), A_n is the amplitude of the nth element, Φ_n is the phase of the nth element, L is the distance between the $x - y$ plane and the $\sigma - \zeta$ plane, and ω_0 is the waist width of the incident beam.

There are two ways to suppress grating lobes. One method is to suppress the grating lobes by using a non-periodic structure at the subarray level or the unit level and then use it to spread the lobes' energy. The other method is to suppress the lobe by using a single array element orientation map. The following subsections describe some of the most critical features of this technique.

C. Optimizing Array Spacing

To obtain an unequally spaced OPA with minimized side lobes level, we apply the modified genetic algorithm to optimize the unequal element distribution for the multi-beam steering. The flow chart for the optimization algorithm is shown in Fig. 2(a). To improve the crossover method of the genetic algorithm, instead of using a single point-to-point crossover, a merit-based crossover is applied. This method can solve the problem of premature convergence, but it will reduce population evolution speed, increase the time complexity of the algorithm, and reduce the algorithm performance. In order to solve this contradiction, a method of accelerating population evolution without destroying population genetic diversity is tried, which is described as follows: after randomly selecting the male parent and the female parent, the crossover method is performed n times to produce 2n individuals, and then the best two individuals are selected from these 2n individuals to join the new population. This not only preserves the genes of the male parent and the female parent, but also greatly improves the average performance of the individuals in the population during the evolutionary process [22]. Here, the sidelobe suppression ratio is used for fitness evaluation, which is represented by the PSLL defined by

$$\mathrm{PSLL} = \max_{\phi=S}\left(\frac{I_{\mathrm{sidelobes}}}{I_{\mathrm{mainlobes}}}\right), \quad (8)$$

where $I_{\mathrm{sidelobes}}$ and $I_{\mathrm{mainlobes}}$ are the power of the sidelobe and the main lobe. S represents the sidelobe interval of the far-field pattern.

First, an unequally spaced linear array model is established, the array aperture is L. Composed of N unequally spaced elements, d_m is the distance between the mth element and the first element. To keep the array aperture constant, there must be array elements at both ends of the linear array with $d_1 = 0$, $d_N = L$. Here, $d_i = x_i + (i-1)d_c$, and we can indirectly transform the individual gene distance interval d_m to x_i and reduce the search space from $[0, L]$ to $[0, L-(N-1)d_c]$. The optimization model of fitness function is defined by

$$\begin{cases} S = \{\theta \mid \theta_{\min} \le \theta \le \theta_0 - \varphi_0 \le \theta \le \theta_{\max}\}; \\ \quad \min\{d_i - d_j\} \ge d_c,\ 1 \le j \le i \le N; \\ x = \{(x_1, x_2, \cdots, x_N) \mid x_1 \le x_2 \le \cdots \le x_N \in [0, L-(N-1)d_c]\}; \\ \quad \min\limits_{x}\ (\mathrm{PSLL}); \end{cases} \quad (9)$$

where θ_0 is the main beam direction, d_c is a constant, indicating the minimum distance interval between two adjacent array elements, which is generally half a wavelength. We optimize the position of the array element by optimizing the value of x to minimize the maximum sidelobe level (PSLL). The fitness evolution curve is shown in Fig. 2(b). In the fitness calculation of each individual in the population, after 115 iterations of optimization, the termination criterion is met, and the optimal result is obtained.

The search area for individuals in the population can be reduced by taking the distance between two adjacent arrays as individual genes. These genes are used to establish an initial population, rank the genes, apply the genes to the population, calculate the degree of adaptation, determine whether the evaluation criteria are met, identify the individual genes that do not meet the requirements, perform selection, and perform crossover and variation genetic operations.

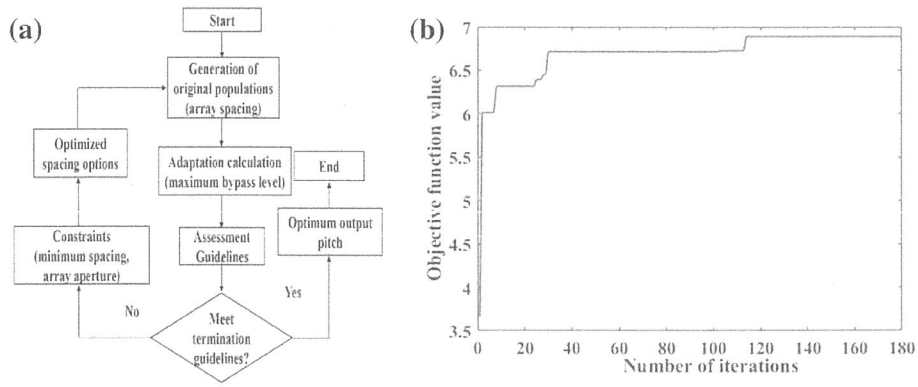

Fig. 2. (a) Flow chart of the optimization algorithm; (b) evolutionary graph of fitness.

3. SIMULATION AND DICUSSION

A. Comparison of One-Dimensional Phased Arrays with Subapertures with Equal and Non-Equal Spacings

To investigate the performance of the proposed method, First, the far-field pattern of a 1D uniform OPA was simulated. In the simulation, the number of OPA elements is 10, the distance between adjacent elements is 0.5λ, λ, 1.5λ, 2λ, and the operating wavelength $\lambda = 1.064$ μm. All elements at the same amplitude and direction, the beam pointing at 0°, the pattern of the array are shown in Fig. 3(a). It can be observed that when the distance between the array elements is greater than half the wavelength ($d > \lambda/2$), the grating lobes equivalent to the main lobe will appear, which is basically consistent with the theory. This means that it is impossible to distinguish the signal incidence direction according to the beam output, and we try to avoid grating lobes when designing the phased array matrix and beam. Meanwhile, OPAs with different array element spacings can obtain different main beams under the same observation direction.

The relationship between beam width, wavelength, and number of array elements is shown in Fig. 3(b). The larger the array element spacing, the narrower the main beam. This is because when the number of array elements is constant, the distance between the array elements will increase the aperture of the OPA array, resulting in a narrower main beam, and the resolution will also increase.

Simulations of the far-field pattern in one- dimension (1D) with unequal spacing were carried out to validate the performance. Assuming that the amplitude for each element is the same, the spacing between adjacent array elements is optimized between 1.5 and 3.5 μm (1.5λ to 3.5λ). A set of solutions is obtained after optimizing the parameters according to the array orientation image's maximum parametric level performance. The far-field intensity of an unequally spaced OPA with a beam angle of 0° is investigated. For an unequally spaced OPA of which the element distribution is optimized by the modified genetic algorithm, the far-field pattern is shown in Figs. 4(a) and 4(b), where the grating lobes are suppressed and the PSLL is reduced to 0.28. The 1D and 2D far-field amplitude distributions for equal and unequal spacing are shown in Figs. 4(c) and 4(d). In this case, the optimized distances between adjacent element of a 10-element OPA are 1.5, 1.9, 1.5, 2.1, 2.7, 2.9, 2.4, 1.9, and 2.9 μm. The above results demonstrate that the unequally spaced OPA optimized by GA can effectively suppress grating lobes and enable higher diffraction efficiency. We will use genetic algorithms to optimize the unequally spaced OPA in multi-beam steering.

B. Optimal Design of Dual-Beam Subaperture Arrays

When the number of array elements is large and the array length is much larger than the wavelength, which will cause the main beam to be very narrow, it is difficult to ensure its stability during beam steering control. Divide the array into multiple subapertures to improve the utilization of the array antenna. The subaperture method divides the OPA element into multiple subapertures and independently controls each subaperture to form M different beams. In this paper, for the convenience of research, we take the dual beams as an example to illustrate the principle. As shown in Fig. 5(a1), the 20-element OPA is equally divided into two groups, each of which will form a beam. To achieve two-beam steering through the phase control method, the corresponding linear phase is loaded to each element, and the phase difference superposition method is used to provide a stable phase. The phase difference between adjacent elements is $\Delta\Phi = \frac{2\pi}{\lambda} d_i \sin\theta_s$, where d_i is the adjacent elements' spacing and θ_s is the beam direction. We investigate the far-field pattern of the equally spaced SA with dual-beam steering angle at ±5°. The results are shown in Fig. 5(b), and the maximum grating lobe level is 0.5871. The grating lobes are more obvious, affecting the diffraction efficiency of the main beam. To reduce the grating lobes' level and higher diffraction efficiency, we need to optimize the element spacing of the subaperture array.

To investigate the performance of the modified GA in suppressing the grating lobes of the OPA in multi-beam steering, we performed simulations. In our model, we divided the 20-element OPA into two subapertures of 10 elements for a wavelength of 1.064 μm. The emission amplitudes and directions of all elements are the same. Figure 5(a2) shows the subaperture array with unequally spaced elements distribution. The elements in two subaperture arrays are loaded with a different linear phase pattern.

First of all, for the convenience of research, we define the subaperture array spacing $d_m = 2$ μm. We use the unequally spaced OPA of which the element distribution is optimized by the proposed genetic algorithm with a dual-beam steering angle at ±5°. The results are shown in Fig. 5(c). The grating lobes are suppressed, and there is a PSLL as low as 0.2156, which is much

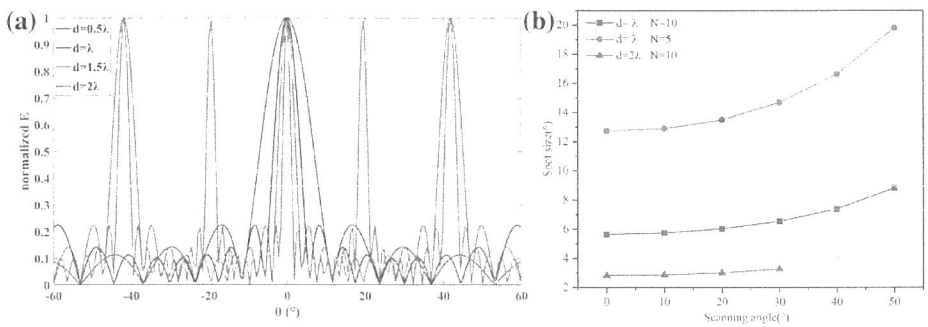

Fig. 3. (a) Far-field beam pattern with 10 elements and spacing 0.5λ, 1λ, 1.5λ, 2λ. (b) The relationship between beam width, wavelength, and number of array elements.

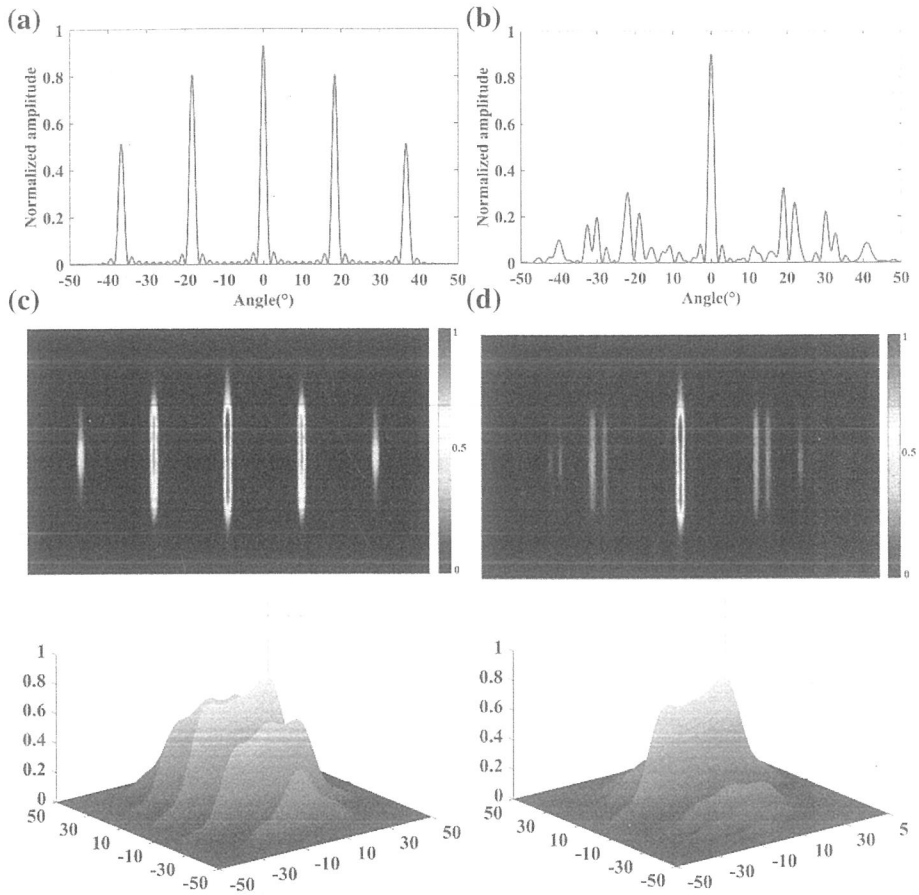

Fig. 4. (a) Equally spaced OPA beam; (b) unequally spaced OPA beam; (c) 2D and 3D far-field amplitude distribution of (a); (d) 2D and 3D far-field amplitude distribution of (b).

lower than the PSLL of 0.5871 in the equally spaced OPA. This means that the optimized unequally spaced SA can suppress the grating lobes' level effectively. Then the results when the beam direction changes are calculated. As shown in Figs. 5(d) and 5(e), we investigate the far-field pattern of the optimized unequally spaced SA when the dual-beam directions are at $\pm 10°$ and $\pm 20°$, and the corresponding PSLLs are 0.2163 and 0.225, respectively. The results show that the grating lobe and side-lobe can be well suppressed by optimizing the array elements' unequal spacing distribution. In addition, we also noticed that the PSLL changes slightly as the beam direction changes, Variation ranges from 0.2 to 0.24. Within the maximum scanning angle, the PSLL of the optimized unequally spaced SA is much smaller than that of the equally spaced SA.

In the research process of unequally spaced SA, due to the particularity of the subaperture array, the subaperture can be individually managed and independently controlled to achieve dual-beam synchronous symmetric scanning and dual-beam asymmetric steering to generate dual-beam asymmetric steering by loading different nonlinear phase modes. Figures 6(a), 6(b), 6(c), and 6(d) show the far-field pattern of the optimized unequally spaced SA when the dual-beam direction is at $(-5°, 20°)$, $(-10°, 20°)$, $(-5°, 25°)$, and $(-10°, 25°)$. The corresponding PSLL is 0.2797, 0.2872, 0.2935, and 0.301, respectively. The results show that the PSLL of the beam asymmetrically steered will be larger than that of the symmetrically steered beam, which is caused by the mutual coupling of the beams.

The control of individual beams is achieved by using SA. An independent phase modulation system is used for individual subarrays. The phase difference between the SA can be adjusted arbitrarily. The maximum scanning angle of a single subarray can reach $52°$ ($d = 2$ μm). Multi-beams allow the array beams' scanning angle to be stitched together, which increases the scanning range and stability of the main beam.

In Fig. 6, we observe that the main lobe width decreases as the beam steering angle increases. Especially in dual-beam asymmetric steering, there is a certain difference in the width of the two main beams, which is basically consistent with the theory. The beam width of the subaperture array is M times that of the original array. It is less affected by the grating lobes of the array grating, and the array beam is more stable.

The relation between PSLL and dual-beam scanning angle and number of array elements is shown in Fig. 7. These will affect the performance of unequally spaced OPAs. The black triangle represents the average of PSLL of the unequally spaced OPA within the maximum scanning angle range. We can see that within the scanning angle, the PSLL of the unequally spaced SA becomes slightly larger as the beam direction angle

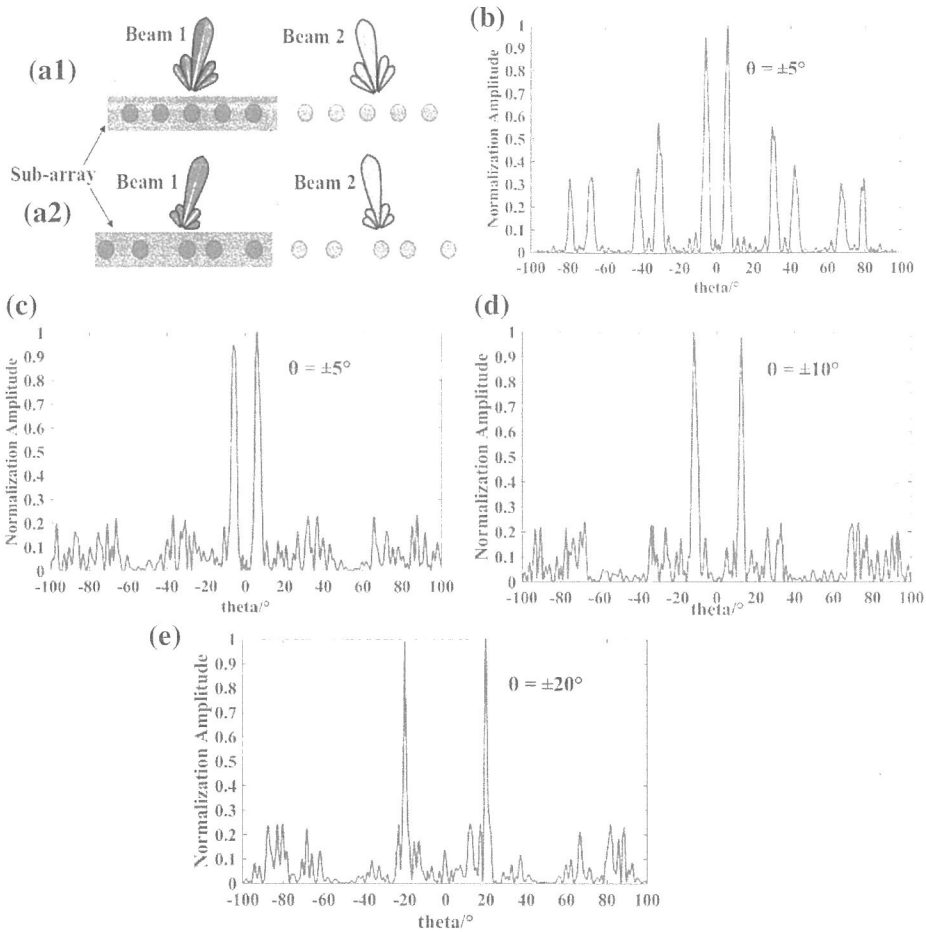

Fig. 5. (a1) and (a2) Diagram of equally spaced and unequally spaced SA; (b) far-field distribution of equally spaced OPAs with $\theta = \pm 5°$. Far-field pattern of optimized unequally spaced OPAs with (c) $\theta = \pm 5°$, (d) $\theta = \pm 10°$, and (e) $\theta = \pm 20°$.

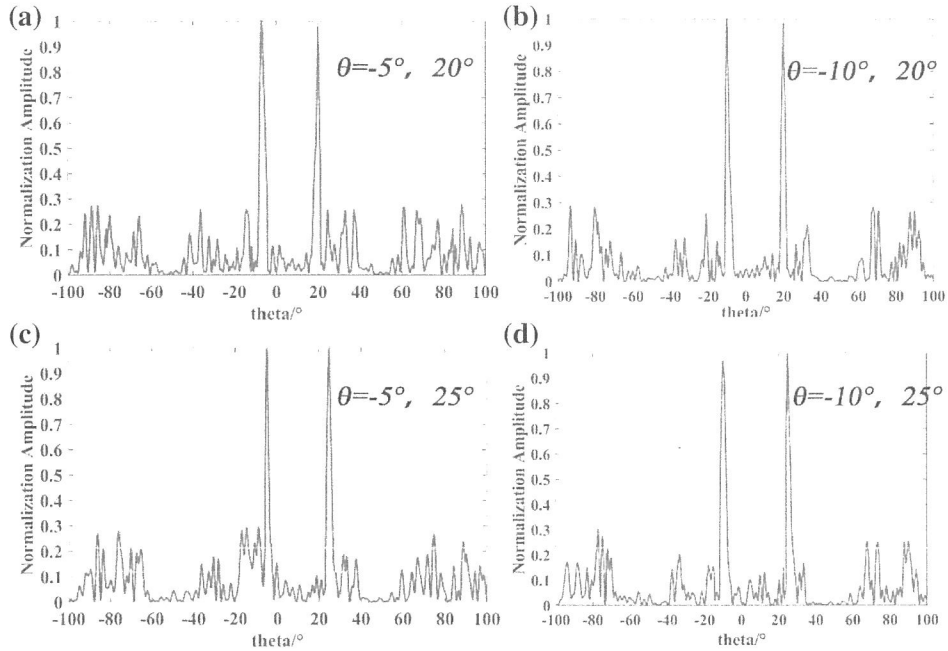

Fig. 6. (a) Far-field distribution of equally spaced OPAs with (a) $\theta = -5°$ and 20°, (b) $\theta = -10°$ and 20°, (c) $\theta = -5°$ and 25°, and (d) $\theta = -10°$ and 25°.

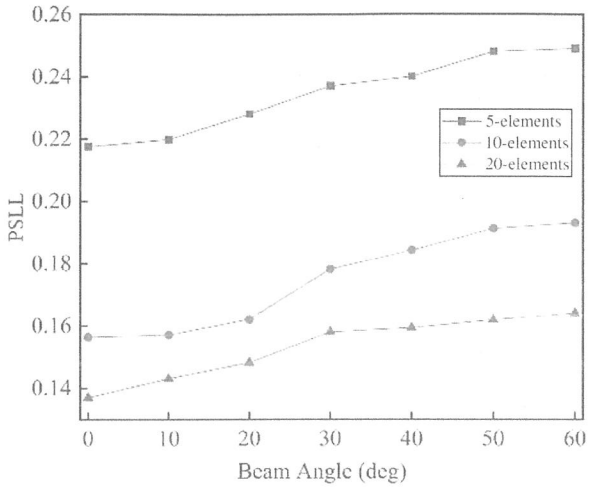

Fig. 7. Diagram of a uniform linear array.

increases, and the lowest of the grating lobes' levels is around the 0° direction. Besides, increasing the space of the SA array can make the PSLL worse. When the number of elements is increased from 5 to 20, the PSLL will become better and the beam width will be narrower, resulting in better directivity and resolution, but the beam stability will be reduced. Therefore, in array design, the number of components and subaperture spacing needs to be weighed against environmental variables and system complexity.

4. CONCLUSION

In this paper, we have proposed and investigated the SA technology to achieve multi-beam low grating lobe steering, and we used modified genetic algorithms to optimize the array element spacing to achieve grating lobe suppression of the OPA. The results show that the grating lobe level of the 10-element subaperture array after optimizing the array element spacing is reduced from 36.7% to 12.3% in ±5°, and dual-beam asymmetric scanning can also be realized. In addition, we have studied how different numbers of subaperture array elements and subaperture array spacings will affect the PSLL and main beam width of the beam. Although a larger scanning angle will increase the PSLL, the PSLL remains at a lower range in the entire scanning range.

Funding. National Natural Science Foundation of China (61675200).

Disclosures. The authors declare that there are no conflicts of interest related to this paper.

Data Availability. Data underlying the results presented in this paper are not publicly available at this time but may be obtained from the authors upon reasonable request.

REFERENCES

1. J. Montoya, A. Sanchez-Rubio, R. Hatch, and H. Payson, "Optical phasedarray ladar," Appl. Opt. **53**, 7551–7555 (2014).
2. A. B. Meinel and M. P. Meinel, "Optical phased array configuration for an extremely large telescope," Appl. Opt. **43**, 601–607 (2004).
3. P. F. McManamon, T. A. Dorschner, D. L. Corkum, L. J. Friedman, D. S. Hobbs, M. Holz, S. Liberman, H. Q. Nguyen, D. P. Resler, R. C. Sharp, and E. A. Watson, "Optical phased array technology," Proc. IEEE **84**, 268–298 (1996).
4. S. Serati, H. Masterson, and A. Linnenberger, "Beam combining using a phased array of phased arrays (papa)," in *IEEE Aerospace Conference Proceedings* (IEEE, 2004), Vol. **3**.
5. A. N. Sousa, I. A. Alimi, R. M. Ferreira, A. Shahpari, M. Lima, P. P. Monteiro, and A. L. Teixeira, "Real-time dual-polarization transmission based on hybrid optical wireless communications," Opt. Fiber Technol. **40**, 114–117 (2018).
6. Y. Litinskaya, A. Alexandrin, K. Lemberg, S. Polenga, and Y. Salomatov, "Phased array antenna with combined electronical and mechanical beam steering for satellite networks," in *International Siberian Conference on Control and Communications (SIBCON)* (IEEE, 2013), pp. 1–3.
7. T. Stephens, W. R. Davis, Jr., and S. E. Forman, "Full aperture mechanical beam steering," Proc. SPIE **783**, 21–28 (1987).
8. M. Jarrahi, R. F. W. Pease, D. A. Miller, and T. H. Lee, "Optical switching based on high-speed phased array optical beam steering," Appl. Phys. Lett. **92**, 014106 (2008).
9. B. Smith, B. Hellman, A. Gin, A. Espinoza, and Y. Takashima, "Single chip lidar with discrete beam steering by digital micromirror device," Opt. Express **25**, 14732–14745 (2017).
10. R. Bonjour, M. Singleton, P. Leuchtmann, and J. Leuthold, "Comparison of steering angle and bandwidth for various phased array antenna concepts," Opt. Commun. **373**, 35–43 (2016).
11. J. K. Doylend, M. Heck, J. T. Bovington, J. D. Peters, L. Coldren, and J. Bowers, "Two-dimensional free-space beam steering with an optical phased array on silicon-on-insulator," Opt. Express **19**, 21595–21604 (2011).
12. C. Tsokos, E. Mylonas, P. Groumas, V. Katopodis, L. Gounaridis, R. B. Timens, R. M. Oldenbeuving, C. G. Roeloffzen, H. Avramopoulos, and C. Kouloumentas, "Analysis of a multibeam optical beamforming network based on Blass matrix architecture," J. Lightwave Technol. **36**, 3354–3372 (2018).
13. M. V. Drummond, V. C. Duarte, A. Albuquerque, R. N. Nogueira, L. Stampoulidis, G. Winzer, L. Zimmermann, S. Clements, and J. Anzalchi, "Dimensioning of a multibeam coherent photonic beamformer fed by a phased array antenna," Opt. Express **26**, 6158–6171 (2018).
14. J. L. Pita, I. Aldaya, O. J. Santana, P. Dainese, and L. H. Gabrielli, "Side-lobe level reduction in bio-inspired optical phased-array antennas," Opt. Express **25**, 30105–30114 (2017).
15. W. S. Rabinovich, P. G. Goetz, M. W. Pruessner, R. Mahon, M. S. Ferraro, D. Park, E. F. Fleet, and M. J. DePrenger, "Two-dimensional beam steering using a thermo-optic silicon photonic optical phased array," Opt. Eng. **55**, 111603 (2016).
16. J. Sun, E. Timurdogan, A. Yaacobi, E. S. Hosseini, and M. R. Watts, "Largescale nanophotonic phased array," Nature **493**, 195–199 (2013).
17. D. Kwong, A. Hosseini, Y. Zhang, and R. T. Chen, "1× 12 unequally spaced waveguide array for actively tuned optical phased array on a silicon nanomembrane," Appl. Phys. Lett. **99**, 051104 (2011).
18. T. Komljenovic, R. Helkey, L. Coldren, and J. E. Bowers, "Sparse aperiodic arrays for optical beam forming and lidar," Opt. Express **25**, 2511–2528 (2017).
19. S. S. Yin, J. H. Kim, F. Wu, P. Ruffin, and C. F. Luo, "Ultra-fast speed, low grating lobe optical beam steering using unequally spaced phased array technique," Opt. Commun. **270**, 41–46 (2007).
20. B. Zhang, Y. Liu, Z. Zhao, and P. Yan, "Multi-beam steering with low grating lobes using optimized unequally spaced phased array," Opt. Commun. **427**, 48–53 (2018).
21. D. Zhang, F. Zhang, and S. Pan, "Grating-lobe-suppressed optical phased array with optimized element distribution," Opt. Commun. **419**, 47–52 (2018).
22. Y. Liu, Z. Hao, L. Wang, B. Xiong, C. Sun, J. Wang, H. Li, Y. Han, and Y. Luo, "A single-chip multi-beam steering optical phased array: design rules and simulations," Opt. Express **29**, 7049–7059 (2021).
23. R. Di Leonardo, F. Ianni, and G. Ruocco, "Computer generation of optimal holograms for optical trap arrays," Opt. Express **15**, 1913–1922 (2007).

24. R. L. Eriksen, P. C. Mogensen, and J. Glückstad, "Multiple-beam optical tweezers generated by the generalized phase-contrast method," Opt. Lett. **27**, 267–269 (2002).
25. F. Xiao and L. Kong, "Optical multi-beam forming method based on a liquid crystal optical phased array," Appl. Opt. **56**, 9854–9861 (2017).
26. A. Calà Lesina, D. Goodwill, E. Bernier, L. Ramunno, and P. Berini, "On the performance of optical phased array technology for beam steering: effect of pixel limitations," Opt. Express **28**, 31637–31657 (2020).